UNIVERSITÄT AUGSBURG
Universitätsbibliothek

OPEN ACCESS
OPUS AUGSBURG

Photoemission electron microscopy of exciton–polaritons in thin WSe2 waveguides

Tobias Eul, Miwan Sabir, Victor DeManuel-Gonzalez, Florian Diekmann, Kai Rossnagel, Michael Bauer

Angaben zur Veröffentlichung / Publication details:

Eul, Tobias, Miwan Sabir, Victor DeManuel-Gonzalez, Florian Diekmann, Kai Rossnagel, and Michael Bauer. 2025. "Photoemission electron microscopy of exciton–polaritons in thin WSe2 waveguides." *ACS Photonics* 12 (7): 3484–91. https://doi.org/10.1021/acsphotonics.5c00290.

Nutzungsbedingungen / Terms of use:

CC BY 4.0

Dieses Dokument wird unter folgenden Bedingungen zur Verfügung gestellt: / This document is made available under these conditions:
CC-BY 4.0: Creative Commons: Namensnennung
Weitere Informationen finden Sie unter: / For more information see:
https://creativecommons.org/licenses/by/4.0/deed.de

ACS Photonics

Open Access

This article is licensed under CC-BY 4.0

pubs.acs.org/journal/apchd5

Article

Photoemission Electron Microscopy of Exciton−Polaritons in Thin WSe_2 Waveguides

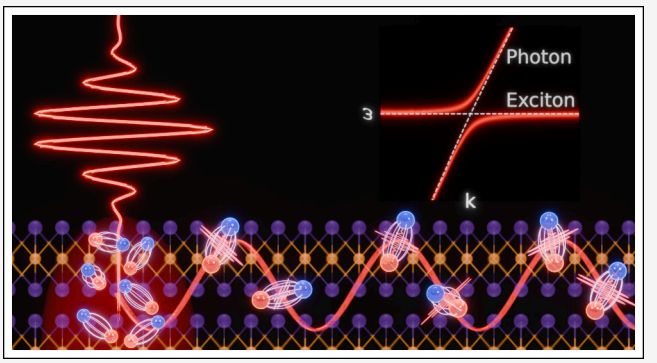
Tobias Eul,* Miwan Sabir, Victor DeManuel-Gonzalez, Florian Diekmann, Kai Rossnagel, and Michael Bauer

Cite This: *ACS Photonics* 2025, 12, 3484−3491

Read Online

ACCESS | Metrics & More | Article Recommendations | Supporting Information

ABSTRACT: Exciton−polaritons emerging from the interaction of photons and excitons in the strong coupling regime are intriguing quasiparticles for the potential exchange of energy during light−matter interaction processes, such as light harvesting. The coupling causes an energy anticrossing in the photon dispersion centered around the exciton resonance, i.e., a Rabi splitting between a lower and upper energetic branch. The size of this splitting correlates with the coupling strength between the exciton and photonic modes. In this work, we investigate this coupling between excitons and photonic waveguide modes excited simultaneously in thin-film flakes of the transition-metal dichalcogenide WSe_2. Using a photoemission electron microscope, we are able to extract the dispersion of the transverse electric and magnetic modes propagating through these flakes as well as extract the energy splitting. Ultimately, our findings provide a basis for the investigation of the propagation of exciton−polaritons in the time-domain via time-resolved photoemission.



KEYWORDS: *light−matter interaction, strong coupling, exciton−polaritons, photoemission electron microscopy, WSe_2*

INTRODUCTION

Excitons, bound electron−hole pairs, are the focus of numerous experimental and theoretical research efforts based on their potential for light-driven energy harvesting. From the many semiconducting materials exhibiting excitonic resonances, transition-metal dichalcogenides (TMDC) have garnered special interest in recent years since they exhibit excitons with large binding energies.[1−4] Embedding TMDC films or even monolayers within micrometer-sized cavities creates a suitable environment for a strong interaction between excitons and photons.[5−10] This interaction facilitates the formation of the light−matter quasiparticle termed exciton−polaritons.[11,12] Its hybrid nature promises new avenues for energy exchange between light and matter and thus new technological developments.

The transfer of energy via the propagation of such a quasiparticle is especially interesting. Therefore, the interaction of excitons with propagating light modes rather than spatially confined cavity photons may provide another suitable environment for exciton−polaritons. Essentially, thin films of TMDC materials themselves host the necessary waveguiding modes, which are able to interact with the intrinsic exciton resonances.[13] Recent near-field studies involving scanning-near field microscopy (SNOM)[14,15] as well as cathode luminescence (CL)[16] focused on this particular approach for exciton−polaritons and discussed their spectroscopic signatures in thin films of WSe_2 and $MoSe_2$. The dispersion of these polaritons exhibits a distinct energy anticrossing centered around the exciton resonance, as illustrated in Figure 1(a).

Photoemission electron microscopy (PEEM) is another experimental technique that demonstrates significant sensitivity to the electric near-field and surface waves in both metallic[17−26] and photonic materials.[27−33] Furthermore, it is possible to measure dispersion relations of these propagating modes by tuning the wavelength of the exciting laser.[27,34−36] The direct imaging of the surface in PEEM in combination with pump−probe excitation schemes additionally facilitates tracing the propagation of waves and quasiparticles along the surface in the time domain.[21,37−39] This makes it a promising method for tracing the propagation of exciton−polaritons in real-time. Ultimately, time-resolved PEEM may even reveal highly local information on the energy transfer, i.e., the Rabi oscillation, between exciton and waveguide mode on an ultrafast time scale.

Received: February 5, 2025
Revised: May 27, 2025
Accepted: May 28, 2025
Published: June 9, 2025



ACS Publications

© 2025 The Authors. Published by American Chemical Society

https://doi.org/10.1021/acsphotonics.5c00290
ACS Photonics 2025, 12, 3484−3491

Downloaded from pubs.acs.org/apchd5/article-pdf/12/7/3484/4459061/ph5c00290.pdf by UNIV AUGSBURG user on 12 November 2026

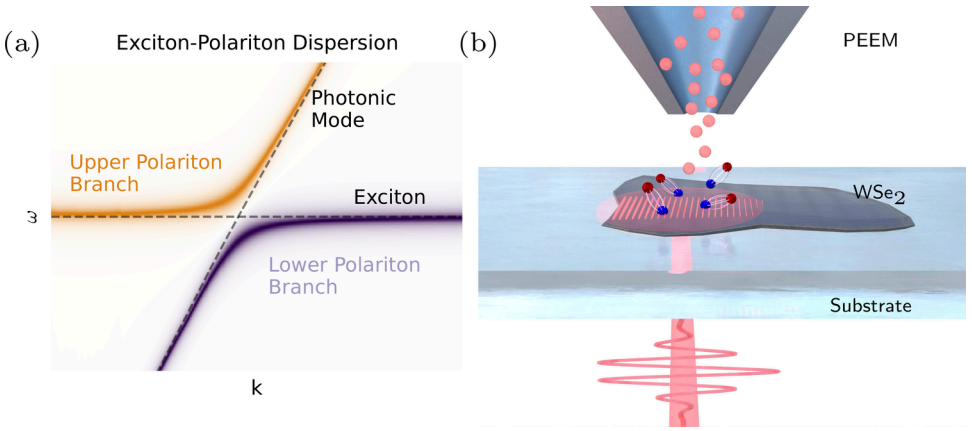


Figure 1. Exciton−polariton dispersion and experimental scheme. (a) Schematic illustration of the exciton−polariton dispersion. (b) Experimental setup with thin WSe_2 flakes situated on a transparent glass substrate. A laser illuminates the flake from the bottom, where it excites the exciton−polaritons and generates the photoelectrons, which enter the PEEM lens system.

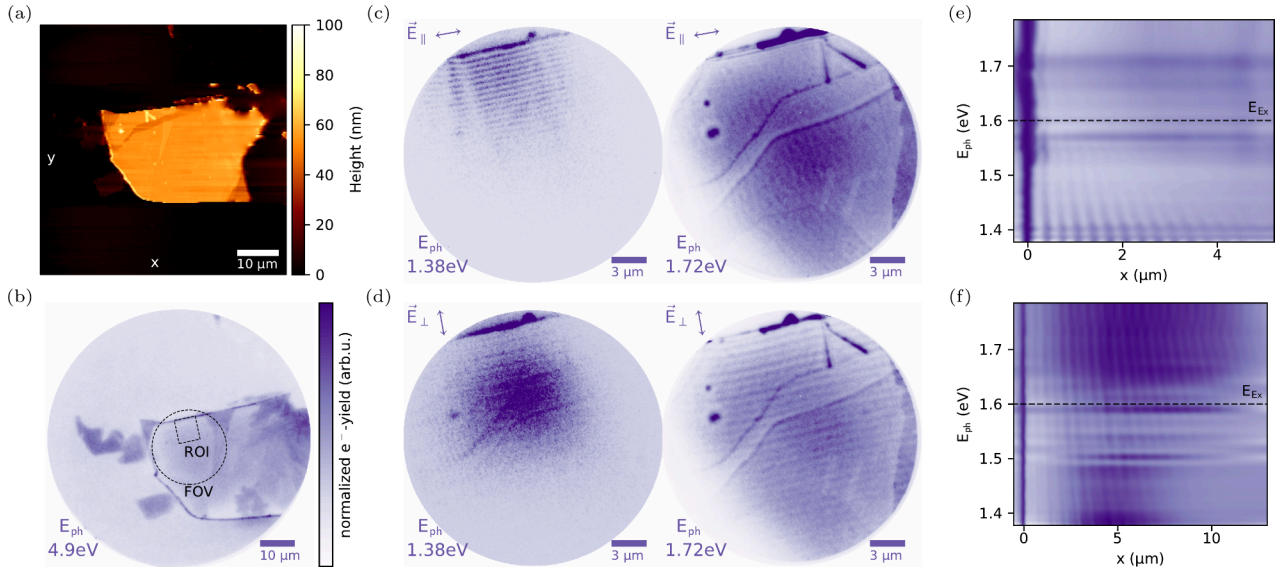


Figure 2. Waveguide mode excitation in WSe_2 investigated using PEEM. (a) AFM image of a WSe_2 flake with a thickness of approximately 55 nm. (b) PEEM image of the same flake recorded with a photon energy of 4.9 eV. The dashed circle (FOV) indicates the field of view of the detailed measurement in (c) and (d). The dashed square (ROI) indicates the region of interest for the extraction of the wave patterns. (c, d) PEEM images recorded with photon energies of 1.38 eV (left) and 1.72 eV (right) with the polarization parallel and perpendicular to the upper edge of the flake, respectively. (e, f) Extracted wave patterns for parallel and perpendicular polarization as a function of excitation photon energy, respectively. The dashed line indicates the energy E_{Ex} of the A-exciton of WSe_2.

RESULTS AND DISCUSSION

In this work, we demonstrate the capability of the PEEM technique to measure the dispersion relation of exciton−polaritons in thin WSe_2 films and determine the coupling strength between the A-exciton and photonic waveguide modes from this data. Figure 1(b) depicts our experimental geometry. A laser with a tunable center wavelength in the range of 695−900 nm corresponding to photon energies E_{Ph} between 1.38 and 1.78 eV illuminates the TMDC sample from the bottom and allows us to spectrally probe the dispersion around the A exciton in WSe_2 at E_{ex} = 1.6 eV.[14,16] A high electric field accelerates the photoelectrons carrying information on the quasiparticle interactions into the PEEM column. The work function of WSe_2, which must be overcome in the photoemission process, is in the order of 4.3 eV[40] and is considerably higher than our photon energies. We reduce the work function of our samples using a procedure that is customary for the PEEM-method:[25,35,36,41,42] We evaporate a fraction of a monolayer of an alkali metal (K) on the surface until it is low enough to enable the emission of photoelectrons via two-photon photoemission (2PPE). In this limit, we are able to generate photoelectrons with the same laser pulses that excite the exciton−polariton. In principle, our study would also be possible without lowering the work function using three-photon photoemission. We discuss the substantial limitations of this approach in the Supporting Information (SI).

We prepared the WSe_2 flakes on indium−tin oxide (ITO) coated glass substrates via the mechanical exfoliation method. This method yields flakes with clean, flat surfaces and well-defined edges, albeit with varying thicknesses (20−150 nm) and lateral dimensions (5−50 μm). Prior to the PEEM experiments, we measured the thickness of the flakes with an atomic force microscope (AFM). Figure 2(a) shows the AFM image for an exemplary WSe_2 flake, which exhibits a thickness

Downloaded from pubs.acs.org/apchd5/article-pdf/12/7/3484/4245906/1/ph5c00290.pdf by UNIV AUGSBURG user on 12 November 2026

https://doi.org/10.1021/acsphotonics.5c00290
ACS Photonics 2025, 12, 3484−3491

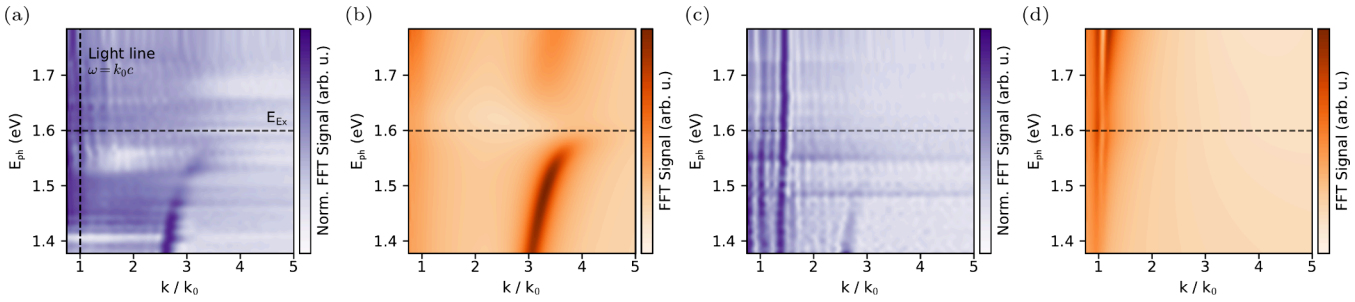


Figure 3. Waveguide mode dispersion. Dispersion curves extracted from the Fourier transformation of measured and simulated wave patterns. The wave numbers k are relative to the wavenumber of light in vacuum k_0. (a, c) Experimental data for the TE- and TM-mode, respectively. (b, d) FDTD simulations for the TE- and TM-mode, respectively. Simulated data were for a flake thickness of 55 nm.

of approximately 55 nm as well as sizes of 30 and 25 μm in the x- and y-direction, respectively. A more detailed description of our methods follows the main text below.

The corresponding PEEM image in Figure 2(b), recorded with a mercury discharge lamp at a photon energy of E_{ph} = 4.9 eV, shows the topography based on work function differences of the substrate and the WSe_2 flake. The dashed circle (FOV) in Figure 2(b) highlights the field of view, where we zoomed in on the sample to get close-up images of the optical near-field of the waveguide modes. The dashed square (ROI) on the other hand marks the region of interest used for the subsequent quantitative analysis. For the experiment, we focus our laser onto the edge of the flake visible at the border of the ROI. Here, the light can couple into different waveguide modes, depending on the in-plane polarization with respect to this edge.

A guided mode propagates through a planar waveguide by internal reflection on the top and bottom interfaces. The polarization dependent phase change upon this reflection determines the character of a mode in the waveguide. Considering the two typical cases of excitation with s- and p-polarized light with respect to the waveguide geometry, two types of modes can be excited in a planar waveguide. S-polarized light couples to transverse electric (TE) modes, where the electric field is perpendicular to the propagation direction. P-polarized light couples to transverse magnetic (TM) modes where the magnetic field is perpendicular to the propagation direction. Since the wave propagates perpendicular to the excitation edge, we couple into a TE-mode for laser polarization parallel to the edge. Similarly, the laser polarization perpendicular to the edge excites a TM-mode.

When these waveguide modes propagate through the flake, its electric field interferes with that of the second photon in the 2PPE-process resulting in a wave pattern in the photoemission contrast on the surface.[20,43] To investigate the dispersion relation of these modes, we excite the flake edge with varying photon energies around the exciton resonance and examine the photoemitted wave patterns.

Figures 2(c,d) shows exemplary images for the photon energies E_{ph} = 1.38 eV and 1.72 eV, respectively, recorded with the polarization parallel (top) and perpendicular (bottom) to the edge. In the case of parallel polarization, i.e. for excitation of a TE-mode, we see a distinct wave pattern for the low photon energy, whereas just one single period of a wave is visible for the large photon energy. This result was to be expected based on the absorption properties of WSe_2 above the energy $E_{Ex} \approx 1.6$ eV of the A-exciton in WSe_2.[14] This absorption influence should be even more apparent in our experiment due to the nonlinear 2PPE excitation scheme. The wave patterns also clearly exhibit different periods, hinting at the dispersion of the photonic mode. For excitation of a TM-mode, on the other hand, the wave pattern remains observable for both photon energies. Figures 2(e,f) illustrates this more clearly in a comparison of the wave patterns at all measured photon energies. For the data comparison, we sum up the intensity in the ROI of the PEEM image along the direction of the edge. As expected, the waves for the TE-mode in (e) show a decreasing propagation length with increasing photon energy. Surprisingly, in the case of the TM-mode in (f) the propagation length does not differ significantly over the measured spectral region. Since the exciton resonance is largely responsible for the absorption in this spectral region, it appears as if the waveguide mode excited via perpendicular polarization does not interact with the exciton, at least for this particular thickness of the flake. This observation will be discussed further below.

The next step of the analysis is to directly extract the dispersion of the photonic modes from the wave patterns. By applying the Fast Fourier Transform (FFT) method to the wave patterns, we can analyze their periods in terms of the amplitude in Fourier space depending on the wavenumber k relative to the wavenumber k_0 of light in free space. Since the wave patterns are not ideal signals with decay and constant offset, we apply a high-pass filter prior to the FFT, which removes low-frequency contributions from the signal. Figure 3 shows the results of this method in dispersion plots consisting of the extracted Fourier signal after normalization to its respective maximum for each photon energy and subsequent interpolation. The normalization is necessary, since the experiment conditions such as focal spot size, intensity, and most importantly for the 2PPE process, the pulse durations vary for each individual photon energy. Figure 3(a) and (c) show the experimental data obtained from the wave patterns in Figure 2(e) and (f), respectively. The dispersion for the TE-mode in Figure 3(a) clearly shows one of the characteristic signatures of strong coupling between exciton and photonic mode, i.e., the lower polariton branch bending in the vicinity of the exciton resonance. The upper branch is not visible due to the strong absorption in this spectral region.

Examining the result for the TM-mode in Figure 3(c), we first notice the same feature as that in Figure 3(a), albeit with a low intensity. This stems from the laser polarization being not perfectly perpendicular to the edge of the WSe_2 flake. More importantly, we see a linear dispersing feature that does not show any deviation from its straight line around the exciton

Downloaded from pubs.acs.org/apchd5/article-pdf/12/7/3484/4245906/1/ph5c00290.pdf by UNIV AUGSBURG user on 12 November 2026

https://doi.org/10.1021/acsphotonics.5c00290
ACS Photonics 2025, 12, 3484−3491

resonance. As already indicated, this mode obviously does not interact with the exciton.

To explain our observations, we additionally simulated the experiment by means of the finite-difference time-domain method[44] and using the optical constants for WSe_2 from ref 45. We use a broadband Gaussian source, which covers the spectral range of the experimental data and focus it on an edge of a thin film of WSe_2. Equivalently, we extracted the electric field wave patterns from a frequency monitor situated in the WSe_2 film and subsequently applied the FFT method. Here, we forego the normalization of the Fourier amplitude for each individual photon energy to retain the information about the absorption. Figure 3(b) and (d) shows the simulated dispersions corresponding to the experimental data in Figure 3(a) and (c), i.e., a thickness of 55 nm and $E_{\parallel}$, $E_{\perp}$, respectively. They reproduce the experiment reasonably well, albeit with a difference in the absolute values of k/k_0, which is probably due to differences in the optical constants for the simulations and actual sample. For an excitation with $E_{\parallel}$ in Figure 3(b), the lower branch disperses similarly to the one obtained from the experiment. However, here we can additionally see the upper branch with a significantly reduced intensity and larger line width than the lower branch. The analysis of the individual electric field components (see Figure S3 in the SI) confirms our initial assignment between laser polarization and the two mode types within the waveguide. The largest contribution to the total electric field, and therefore the dispersion signal, comes from the component parallel to the excitation edge. Since the waveguide mode propagates in the direction perpendicular to the edge, we can attribute the dispersive feature to a transverse electric (TE) mode. Similarly, we determine from the simulation data in Figure 3(d) and Figure S3 that the light with $E_{\perp}$ indeed couples into a transverse magnetic (TM) mode. As in the experiment, the dispersion in this case is a straight line, again without any sign of interaction with the exciton. The experimental data and simulation in Figure 3(c) and (d) also exhibit another feature at $k/k_0 = 1$, i.e., a mode that follows the dispersion of light in free space. This additional feature stems from the excitation source.

Additional simulations in the SI and similar results in ref 14 show that for increasing flake thickness the exciton also starts to couple to the TM-mode. Interestingly, for both the TE- and TM-mode, there seems to be a threshold for the waveguide thickness that determines the coupling to the exciton. For the TE-mode, this thickness threshold lies between 20 and 30 nm, whereas the waveguide needs to be thicker than 60 nm for the TM-mode to couple. When analyzing the electric field localization within the waveguide (see Figures S5 and S7), it becomes clear that the exciton coupling depends on how strongly the light is confined within the waveguide. In the case of the TE-mode, the waveguides become simply too thin. The electric field is still very localized, but too much light resides outside of the waveguide below 30 nm. For the TM-mode, however, the electric field amplitudes starts to delocalize for thicknesses below 60 nm, which is why the threshold is different from the TE-mode.

To summarize, the data show that for this particular thickness of the WSe_2 flake we are able to control the exciton–photon coupling with the laser polarization being the experimental control parameter. We can either couple into the TE-mode for strong coupling or into the TM-mode for a freely propagating waveguide mode.

Ultimately, we are interested in the coupling strength of the exciton–polariton, which can be determined from the energy splitting in the dispersion curve. For this, we examine another WSe_2 flake with a significantly smaller thickness, so that the absorption is overall reduced. As mentioned above, in this thickness range only the TE-mode couples to the exciton. Figure 4(a) shows the PEEM image for this flake recorded at

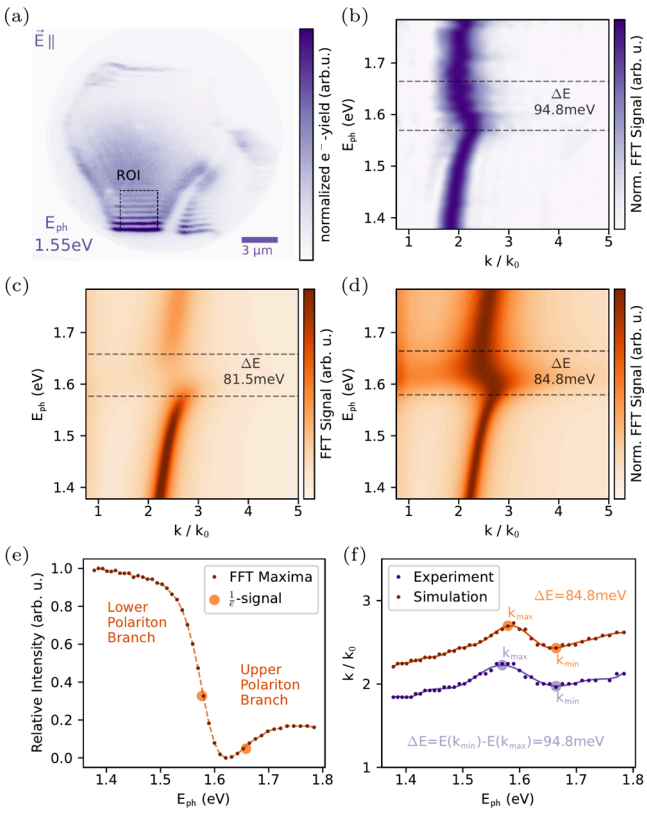


Figure 4. Strong-coupling energy splitting. (a) PEEM image of a WSe_2 flake recorded with a photon energy of 1.55 eV and laser polarization oriented parallel to the bottom edge. The dashed square (ROI) indicates the region of interest for the extraction of the wave patterns. (b) Dispersion of the TE-mode evaluated from the experimental data. (c,d) Simulated dispersion for a thickness of 30 nm without and with normalizing the signal of each individual frequency. (e) Extracted maximum FFT signals from (c) for determining the energy splitting based on exponential reduction of the branch intensities. (f) Extracted maxima positions from (b) and (d) for determining the energy gaps based on turning points in the dispersion.

E_{ph} = 1.55 eV with the polarization of the laser oriented parallel to the excitation edge at the bottom. The dashed square (ROI) marks the region of interest for the analysis of the wave patterns. Since the absorption is now reduced, we can resolve both the lower and the upper branches of the exciton–polariton in the dispersion curve in Figure 4(b). Due to the individual normalization of the signal for each photon energy, we do not see a gap around the exciton resonance. Nevertheless, we can assign an energy splitting between the two branches based on the turning points within the two polariton branches. This becomes more evident when analyzing the corresponding FDTD simulations for a thickness of 30 nm, as shown in Figure 4(c,d).

The two simulated dispersion plots show the same dispersion data without normalization in Figure 4(c) and

Downloaded from pubs.acs.org/apchd5/article-pdf/12/7/3484/4245906/1/ph5c00290.pdf by UNIV AUGSBURG user on 12 November 2026

https://doi.org/10.1021/acsphotonics.5c00290
ACS Photonics 2025, 12, 3484–3491

with normalization of the signal for each photon energy equivalent to the experimental data in Figure 4(d). From the data without normalization, it is possible to extract the energy splitting in a straightforward manner by analyzing the intensity distribution of the two branches. Figure 4(e) shows the relative maximum intensity of the branches extracted for each photon energy. In both branches we determine the point where the intensity has decreased to the $\frac{1}{e}$ fraction. We take the energy difference between these two points as a measure of the energy splitting of the dispersion curve. For the examined flake thickness, the analysis yields an energy splitting of ΔE = 81.5 meV. The dashed lines in Figure 4(c) mark the extracted limits and the splitting. For the normalized data, we evaluate the energy splitting based on the two turning points in the dispersion curve located between the two branches that are clearly visible in Figure 4(d).

For the quantitative analysis, we extract the k/k_0 values of the maximum in the dispersion for each photon energy and approximate this $k(E_{ph})$ relation by applying a Savitzky–Golay filter on the data points. Figure 4(f) shows this relation in orange for the simulated data. The curve shows clear local maxima and minima, which we identify as the k/k_0 values of the turning points. The corresponding photon energies at these points yield a value for the energy splitting of ΔE = 84.4 meV. This value is very close to that extracted from the unnormalized data, which validates this approach. We therefore apply the equivalent procedure to the experimentally determined dispersion curve. The data from this analysis, shown as a blue line in Figure 4(f), yield an energy splitting of ΔE = 94.8 meV for the exciton–polariton.

This value is in good agreement with the results of a SNOM study on exciton–photon coupling in $MoSe_2$ flakes.[15] Conversely, the above-mentioned CL study on WSe_2 flakes[16] discusses larger values of up to 300 meV. This discrepancy stems from two effects present in the CL experiment. First, the excitation with the electron beam in the CL experiment results in much higher exciton densities in the interaction volume with the waveguide mode compared to the light induced excitation used in this study, which enhances the exciton–polariton coupling.[46] Second, electron beams with sufficiently high beam energy generate Cherenkov radiation, which further increases the interaction strength with the excitons.[47]

CONCLUSION

In summary, we studied and analyzed the coupling strength between photonic waveguide modes and the A-exciton in thin-film WSe_2 flakes. By varying the photon energy as well as the polarization of the exciting laser, we were able to extract the dispersion relation of different modes from the near-field wave patterns recorded with PEEM. Additional FDTD simulations reproduced the experimental dispersion curves and provided us another avenue to analyze the strong coupling and the associated energy splitting between the lower and upper polariton branch. The simulations affirmed the nature of the modes, i.e., TE or TM for a polarization parallel or perpendicular to the excitation edge, respectively. With our experiment, we ascertained the challenge in accessing the upper polariton branch using nonlinear photoemission due to a strong absorption in WSe_2 for this spectral region. Nevertheless, we were able to extract the energy splitting from the turning points in the normalized dispersion curve, with ΔE on the order of 100 meV for the exciton–polariton formed from the TE-mode.

In comparison, PEEM provides similar information as the scanning near-field microscopy technique employed in previous work on exciton–polaritons.[14,15] For example, the extracted energy splitting compares well with the splitting of 100 meV observed with SNOM in thin films of $MoSe_2$. While SNOM allows to perform experiment under ambient conditions, PEEM, in combination with varying the laser polarization, is more flexible in selectively exciting the different TE or TM modes. Additionally, the parallel imaging of the surface, in contrast to scanning over it, allows for a faster data acquisition, and therefore facilitates an easier combination with pump–probe techniques for ultrafast time-domain studies. We expect that time-resolved PEEM will provide a new avenue to investigate the propagation of exciton–polaritons as well as the periodic energy exchange between the involved quasiparticles in real time.

EXPERIMENTAL DETAILS

Photoemission Electron Microscope. The photoemission electron microscope (Focus GmbH) consists of an electrostatic lens system, which images the lateral distribution of photoelectrons emitted from the sample surface. An extractor lens situated directly in front of the sample collects the photoemitted electrons with a high voltage electric field, e.g., V_{ext} = 10 kV for this study. The detector is a combination of a multichannel-plate (MCP), which multiplies the photoelectrons, and a phosphor screen, whose illumination is captured by a CCD camera (LaVision). The photoelectrons are detected in an energy integrated manner with a high spatial resolution of $\Delta x \approx 50$ nm. The overall system is contained within an ultrahigh vacuum chamber with pressures typically in the order of $p \leq 5 \times 10^{-10}$ mbar. The system additionally features a wire-shaped alkali metal dispenser (SAES Getters) for the evaporation of small doses of potassium onto sample surfaces.

For the photoexcitation, the sample can be illuminated by laser sources through two different vacuum chamber entrance windows, either under a grazing incidence of 65° or under normal illumination from the back side of the sample. The latter case additionally allows very tight focusing of the laser beam down to 5 μm spot sizes via a lens in close proximity to the sample. More information on this normal incidence configuration can be found in ref 48. Additionally, the PEEM is equipped with a mercury discharge lamp (Focus GmbH) providing continuous wave, unpolarized light with a photon energy of 4.9 eV, which is primarily used for overview images of the sample surface and adjustment based on work function contrasts.

Laser System. Our laser system is a pulsed titanium-sapphire (Ti:Sa) oscillator system (Tsunami, Spectra Physics) operated at a repetition rate of 80 MHz and pumped with P_{pump} = 7.5 W of the second harmonic of a diode pumped neodymium–yttrium vanadate laser (Millennia Pro 10s, Spectra Physics). The central wavelength of the Ti:Sa output is tunable in the range of 700–900 nm. Depending on the output spectrum, the duration of the outgoing laser pulses varies in the range of 100–130 fs. Similarly, the output power lies within the range of P_{out} = 0.5–1 W. Between the laser system and the PEEM no additional pulse compression was used because the priority of the experiment was a stable pointing of the beam onto the sample while tuning the central

Downloaded from pubs.acs.org/apchd5/article-pdf/12/7/3484/4245906/ph5c00290.pdf by UNIV AUGSBURG user on 12 November 2026

https://doi.org/10.1021/acsphotonics.5c00290
ACS Photonics 2025, 12, 3484–3491

wavelength of the laser. Two lenses used as a telescope, the vacuum chamber entrance window, an in-vacuum lens, and a half wave plate are present in the beam path and lengthen our pulse duration upon beam transmission. All reflective optics used were optimized for minimal group delay dispersion.

Alignment of sample and laser. The half wave plate is situated directly before the vacuum chamber entrance window to control the in-plane polarization of the laser upon illuminating the sample under normal incidence. The alignment of the laser with respect to the WSe_2 flake is very crucial due to the rather small spot sizes of the laser in the order of 5−20 μm at the sample. Ideally, the center of the beam should be on the excitation edge of the flake to achieve the best coupling to the waveguide mode. Unfortunately, this would result in a very strong overexposure of the edge in the photoemission signal and a very low contrast in the rest of the field of view. Therefore, we position the spot in a way that enough of the Gaussian profile clips the excitation edge to launch the waveguide mode while the intensity maximum is in the center of the field of view. This skews the overall intensity of the wave and makes it appear as if the waves decay away from the center of the field of view. Depending on the photon energy, this effect is more or less pronounced, as is evident from Figure 2. This is why we apply a high pass Fourier filter to the PEEM images along the propagation direction and normalize the data for each photon energy individually.

Sample Fabrication. Single crystals of 2Hb-WSe_2 were grown by iodine vapor transport. High-purity tungsten wire and selenium pellets were sealed at one end of evacuated quartz ampules (inner diameter 12 mm, length 200 mm) in a near stoichiometric ratio with approximately 15% selenium excess (3 mg/cm^3) together with iodine granules (5 mg/cm^3). The ampules were subjected to a temperature gradient of 60 °C, with the hotter end containing the starting materials at 900 °C. The growth time for crystals forming near the colder end was 900 h. The size of the crystals were up to 5 × 5 mm^2 in area and 0.1 mm thick. The doping of the semiconducting samples is typically p-type.[49] We prepared our samples via mechanical exfoliation of the bulk WSe_2 crystal. For this, we press a semiconductor wafer dicing tape on top of the bulk and remove the topmost layers. With a second strip of this tape, we repeat the process on the material stuck on the first tape and afterward the same with a third tape. Finally, we press the third tape on top of our glass substrate to transfer the WSe_2 layers. The glass substrate (Präzisions Glas and Optik GmbH) is a standard soda lime glass with a thickness of 1.1 mm covered with a few nano meters of a SiO_2 passivation layer. On top of this is a sputter deposited thin film of indium−tin oxide with a thickness of 21 nm and a resistance of 100 Ω. Prior to the PEEM experiments, we evaporated a fraction of a monolayer of potassium onto the sample surface to reduce the work function. For this, we operate the K-dispenser at I = 5.7 A for 60 s from a distance of approximately 5.5 cm to the sample. Over time, and especially after illumination with the laser, the potassium level on the WSe_2 surface decreases and needs to be refreshed. This effect occurs faster for illumination at the exciton resonance.

Finite-Difference Time Domain Simulations. The simulation environment spans a volume of 25 μm × 3 μm × 4 μm with a uniform 20 nm × 20 nm × 100 nm mesh grid in the region of the waveguide. The mesh step in the z-direction is quite large to reduce simulation size and time. We ensured its validity by reproducing the results of exemplary simulations with Δz = 4 nm. The environment is surrounded by perfect-matching layer boundaries, and the total run time per simulation is 200 fs. The WSe_2 waveguide sits on top of a 21 nm thin indium−tin oxide film and a glass substrate filling the simulation environment in the negative z-direction. Its excitation edge is located at x = −4 μm, with propagation in the positive x-direction. All materials fill the environment in the y-direction. The source is given by a Gaussian beam with a waist radius of 5 μm at the excitation edge of the waveguide. Its spectrum is centered around 800 nm with a full width at half-maximum of 100 nm and a temporal width of about 16 fs. A 2D-field monitor located at the top surface of the WSe_2 waveguide records the electric field components in the wavelength range of 650−950 nm.

Atomic Force Microscope. We used a commercial atomic force microscope (Veeco, Nanoscope V) and tip (Budget-sensors, TAP 150). The AFM is installed on an antivibration table. The aluminum coated tip has a resonance frequency of about 150 kHz and we measure the height of the WSe_2 flakes in tapping mode.

■ ASSOCIATED CONTENT

Data Availability Statement

The data that support the findings of this study are openly available in Zenodo at 10.5281/zenodo.14168816.

Supporting Information

The Supporting Information is available free of charge at https://pubs.acs.org/doi/10.1021/acsphotonics.5c00290.

Additional results measured in the 3PPE regime, and additional simulations of the electric field components, thickness-dependent dispersion, and the field localizations in the waveguide (PDF)

■ AUTHOR INFORMATION

Corresponding Author

Tobias Eul − *Institute of Experimental and Applied Physics, Kiel University, 24098 Kiel, Germany;* orcid.org/0000-0002-7362-6448; Email: eul@physik.uni-kiel.de

Authors

Miwan Sabir − *Institute of Experimental and Applied Physics, Kiel University, 24098 Kiel, Germany*

Victor DeManuel-Gonzalez − *Institute of Experimental and Applied Physics, Kiel University, 24098 Kiel, Germany*

Florian Diekmann − *Institute of Experimental and Applied Physics, Kiel University, 24098 Kiel, Germany;* orcid.org/0000-0002-8877-710X

Kai Rossnagel − *Institute of Experimental and Applied Physics, Kiel University, 24098 Kiel, Germany; Kiel Nano, Surface and Interface Science KiNSIS, Kiel University, 24118 Kiel, Germany;* orcid.org/0000-0001-5107-0090

Michael Bauer − *Institute of Experimental and Applied Physics, Kiel University, 24098 Kiel, Germany; Kiel Nano, Surface and Interface Science KiNSIS, Kiel University, 24118 Kiel, Germany;* orcid.org/0000-0002-4391-9899

Complete contact information is available at: https://pubs.acs.org/10.1021/acsphotonics.5c00290

Author Contributions

M.B. conceived the ideas and designed the experiments. T.E. carried out the PEEM experiments and the FDTD simulations and is responsible for the data evaluation. F.D. and K.R.

Downloaded from pubs.acs.org/apchd5/article-pdf/12/7/3484/4245906/ph5c00290.pdf by UNIV AUGSBURG user on 12 November 2026

synthesized the WSe_2 crystals. M.S. performed the mechanical exfoliation of the WSe_2 flakes onto the ITO substrates. V.D.G. carried out the AFM measurements. T.E. and M.B. wrote the manuscript.

Funding

The PEEM study and the sample growth were supported by the German Research Foundation (DFG) through Projects 499426961 and 434434223 (CRC 1461), respectively.

Notes

The authors declare no competing financial interest.

■ ACKNOWLEDGMENTS

The authors acknowledge Prof. Dr. Nahid Talebi for discussions regarding the thickness-dependent coupling and the comparison of the PEEM and CL data.

■ REFERENCES

(1) Cheiwchanchamnangij, T.; Lambrecht, W. R. L. Quasiparticle band structure calculation of monolayer, bilayer, and bulk MoS_2. *Phys. Rev. B* **2012**, *85*, 205302.
(2) Chernikov, A.; Berkelbach, T. C.; Hill, H. M.; Rigosi, A.; Li, Y.; Aslan, B.; Reichman, D. R.; Hybertsen, M. S.; Heinz, T. F. Exciton Binding Energy and Nonhydrogenic Rydberg Series in Monolayer WS_2. *Phys. Rev. Lett.* **2014**, *113*, 076802.
(3) Zhu, B.; Chen, X.; Cui, X. Exciton Binding Energy of Monolayer WS2. *Sci. Rep.* **2015**, *5*, 9218.
(4) Wang, G.; Chernikov, A.; Glazov, M. M.; Heinz, T. F.; Marie, X.; Amand, T.; Urbaszek, B. Colloquium: Excitons in atomically thin transition metal dichalcogenides. *Rev. Mod. Phys.* **2018**, *90*, 021001.
(5) Dufferwiel, S.; Schwarz, S.; Withers, F.; Trichet, A. A. P.; Li, F.; Sich, M.; Del Pozo-Zamudio, O.; Clark, C.; Nalitov, A.; Solnyshkov, D. D.; Malpuech, G.; Novoselov, K. S.; Smith, J. M.; Skolnick, M. S.; Krizhanovskii, D. N.; Tartakovskii, A. I. Exciton-polaritons in van der Waals heterostructures embedded in tunable microcavities. *Nat. Commun.* **2015**, *6*, 8579.
(6) Liu, X.; Galfsky, T.; Sun, Z.; Xia, F.; Lin, E.-c.; Lee, Y.-H.; Kéna-Cohen, S.; Menon, V. M. Strong light-matter coupling in two-dimensional atomic crystals. *Nat. Photonics* **2015**, *9*, 30−34.
(7) Lundt, N.; Klembt, S.; Cherotchenko, E.; Betzold, S.; Iff, O.; Nalitov, A. V.; Klaas, M.; Dietrich, C. P.; Kavokin, A. V.; Höfling, S.; Schneider, C. Room-temperature Tamm-plasmon exciton-polaritons with a WSe2 monolayer. *Nat. Commun.* **2016**, *7*, 13328.
(8) Flatten, L. C.; He, Z.; Coles, D. M.; Trichet, A. A. P.; Powell, A. W.; Taylor, R. A.; Warner, J. H.; Smith, J. M. Room-temperature exciton-polaritons with two-dimensional WS2. *Sci. Rep.* **2016**, *6*, 33134.
(9) Liu, X.; Bao, W.; Li, Q.; Ropp, C.; Wang, Y.; Zhang, X. Control of Coherently Coupled Exciton Polaritons in Monolayer Tungsten Disulphide. *Phys. Rev. Lett.* **2017**, *119*, 027403.
(10) Chen, Y.-J.; Cain, J. D.; Stanev, T. K.; Dravid, V. P.; Stern, N. P. Valley-polarized exciton-polaritons in a monolayer semiconductor. *Nat. Photonics* **2017**, *11*, 431−435.
(11) Weisbuch, C.; Nishioka, M.; Ishikawa, A.; Arakawa, Y. Observation of the coupled exciton-photon mode splitting in a semiconductor quantum microcavity. *Phys. Rev. Lett.* **1992**, *69*, 3314−3317.
(12) Gibbs, H. M.; Khitrova, G.; Koch, S. W. Exciton−polariton light-semiconductor coupling effects. *Nat. Photonics* **2011**, *5*, 273−273.
(13) Zong, X.; Li, L.; Li, L.; Yu, K.; Liu, Y. Self-hybridized exciton-polaritons in thin films of transition metal dichalcogenides for narrowband perfect absorption. *Opt. Express* **2023**, *31*, 18545−18554.
(14) Fei, Z.; Scott, M. E.; Gosztola, D. J.; Foley, J. J.; Yan, J.; Mandrus, D. G.; Wen, H.; Zhou, P.; Zhang, D. W.; Sun, Y.; Guest, J. R.; Gray, S. K.; Bao, W.; Wiederrecht, G. P.; Xu, X. Nano-optical imaging of WSe_2 waveguide modes revealing light-exciton interactions. *Phys. Rev. B* **2016**, *94*, 081402.
(15) Hu, F.; Luan, Y.; Scott, M. E.; Yan, J.; Mandrus, D. G.; Xu, X.; Fei, Z. Imaging exciton−polariton transport in MoSe2 waveguides. *Nat. Photonics* **2017**, *11*, 356−360.
(16) Taleb, M.; Davoodi, F.; Diekmann, F. K.; Rossnagel, K.; Talebi, N. Charting the Exciton−Polariton Landscape of WSe2 Thin Flakes by Cathodoluminescence Spectroscopy. *Advanced Photonics Research* **2022**, *3*, 2100124.
(17) Kubo, A.; Onda, K.; Petek, H.; Sun, Z.; Jung, Y. S.; Kim, H. K. Femtosecond Imaging of Surface Plasmon Dynamics in a Nanostructured Silver Film. *Nano Lett.* **2005**, *5*, 1123−1127.
(18) Meyer zu Heringdorf, F.-J.; Chelaru, L.; Möllenbeck, S.; Thien, D.; Horn-von Hoegen, M. Femtosecond photoemission microscopy. *Surf. Sci.* **2007**, *601*, 4700−4705.
(19) Leißner, T.; Thilsing-Hansen, K.; Lemke, C.; Jauernik, S.; Kjelstrup-Hansen, J.; Bauer, M.; Rubahn, H.-G. Surface Plasmon Polariton Emission Prompted by Organic Nanofibers on Thin Gold Films. *Plasmonics* **2012**, *7*, 253−260.
(20) Kahl, P.; Wall, S.; Witt, C.; Schneider, C.; Bayer, D.; Fischer, A.; Melchior, P.; Horn-von Hoegen, M.; Aeschlimann, M.; Meyer zu Heringdorf, F.-J. Normal-Incidence Photoemission Electron Microscopy (NI-PEEM) for Imaging Surface Plasmon Polaritons. *Plasmonics* **2014**, *9*, 1401−1407.
(21) Spektor, G.; Kilbane, D.; Mahro, A. K.; Frank, B.; Ristok, S.; Gal, L.; Kahl, P.; Podbiel, D.; Mathias, S.; Giessen, H.; zu Heringdorf, F.-J. M.; Orenstein, M.; Aeschlimann, M. Revealing the subfemtosecond dynamics of orbital angular momentum in nanoplasmonic vortices. *Science* **2017**, *355*, 1187−1191.
(22) Joly, A. G.; El-Khoury, P. Z.; Hess, W. P. Spatiotemporal Imaging of Surface Plasmons Using Two-Color Photoemission Electron Microscopy. *J. Phys. Chem. C* **2018**, *122*, 20981−20988.
(23) Dąbrowski, M.; Dai, Y.; Petek, H. Ultrafast Photoemission Electron Microscopy: Imaging Plasmons in Space and Time. *Chem. Rev.* **2020**, *120*, 6247−6287.
(24) Großmann, M.; Black, M.; Jaruschewski, J.; Klick, A.; Leißner, T.; Fiutowski, J.; Rubahn, H.-G.; Bauer, M. Micro-spectroscopy of Buried Short-Range Surface Plasmon Polaritons Supported by Thin Polycrystalline Gold Films. *Plasmonics* **2021**, *16*, 737−746.
(25) Davis, T. J.; Janoschka, D.; Dreher, P.; Frank, B.; zu, F.-J. M.; Giessen, H. Ultrafast vector imaging of plasmonic skyrmion dynamics with deep subwavelength resolution. *Science* **2020**, *368*, eaba6415.
(26) Kilbane, D.; Prinz, E.; Eul, T.; Hartelt, M.; Mahro, A.-K.; Hensen, M.; Pfeiffer, W.; Aeschlimann, M. Plasmonic wavelength-dependent optical switch. *Opt. Express* **2023**, *31*, 9579−9590.
(27) Fitzgerald, J. P. S.; Word, R. C.; Saliba, S. D.; Könenkamp, R. Photonic near-field imaging in multiphoton photoemission electron microscopy. *Phys. Rev. B* **2013**, *87*, 205419.
(28) Word, R. C.; Fitzgerald, J. P. S.; Könenkamp, R. Direct coupling of photonic modes and surface plasmon polaritons observed in 2-photon PEEM. *Opt. Express* **2013**, *21*, 30507−30520.
(29) Fitzgerald, J. P. S.; Word, R. C.; Könenkamp, R. Subwavelength visualization of light in thin film waveguides with photoelectrons. *Phys. Rev. B* **2014**, *89*, 195129.
(30) Aeschlimann, M.; Brixner, T.; Differt, D.; Heinzmann, U.; Hensen, M.; Kramer, C.; Lükermann, F.; Melchior, P.; Pfeiffer, W.; Piecuch, M.; Schneider, C.; Stiebig, H.; Strüber, C.; Thielen, P. Perfect absorption in nanotextured thin films via Anderson-localized photon modes. *Nat. Photonics* **2015**, *9*, 663−668.
(31) Klick, A.; Wagner, R.; Großmann, M.; Kadem, L. F.; Leißner, T.; Rubahn, H.-G.; Selhuber-Unkel, C.; Bauer, M. Detection and characterization of attenuated multimode waveguiding in SiO_2 slabs using photoemission electron microscopy. *Phys. Rev. B* **2018**, *98*, 085128.
(32) Stenmark, T.; Könenkamp, R. Photoemission electron microscopy to characterize slow light in a photonic crystal line defect. *Phys. Rev. B* **2019**, *99*, 205428.
(33) Aeschlimann, M.; Brixner, T.; Fenner, F.; Frisch, B.; Folge, P.; Hartelt, M.; Hensen, M.; Loeber, T. H.; Pfeiffer, W.; Pres, S.; Stannowski, B. Direct imaging of photonic band-edge states in golden

Downloaded from pubs.acs.org/apchd5/article-pdf/12/7/3484/4245906/ph5c00290.pdf by UNIV AUGSBURG user on 12 November 2026

https://doi.org/10.1021/acsphotonics.5c00290
ACS Photonics 2025, 12, 3484−3491

Vogel spirals using photoemission electron microscopy. *J. Opt. Soc. Am. B* **2023**, *40*, B19−B27.
(34) Leißner, T.; Lemke, C.; Fiutowski, J.; Radke, J. W.; Klick, A.; Tavares, L.; Kjelstrup-Hansen, J.; Rubahn, H.-G.; Bauer, M. Morphological Tuning of the Plasmon Dispersion Relation in Dielectric-Loaded Nanofiber Waveguides. *Phys. Rev. Lett.* **2013**, *111*, 046802.
(35) Lemke, C.; Leißner, T.; Klick, A.; Fiutowski, J.; Radke, J. W.; Thomaschewski, M.; Kjelstrup-Hansen, J.; Rubahn, H.-G.; Bauer, M. The complex dispersion relation of surface plasmon polaritons at gold/para-hexaphenylene interfaces. *Appl. Phys. B: Laser Opt.* **2014**, *116*, 585−591.
(36) Hartelt, M.; Terekhin, P. N.; Eul, T.; Mahro, A.-K.; Frisch, B.; Prinz, E.; Rethfeld, B.; Stadtmüller, B.; Aeschlimann, M. Energy and Momentum Distribution of Surface Plasmon-Induced Hot Carriers Isolated via Spatiotemporal Separation. *ACS Nano* **2021**, *15*, 19559−19569.
(37) Kubo, A.; Pontius, N.; Petek, H. Femtosecond Microscopy of Surface Plasmon Polariton Wave Packet Evolution at the Silver/Vacuum Interface. *Nano Lett.* **2007**, *7*, 470−475.
(38) Lemke, C.; Leißner, T.; Jauernik, S.; Klick, A.; Fiutowski, J.; Kjelstrup-Hansen, J.; Rubahn, H.-G.; Bauer, M. Mapping surface plasmon polariton propagation via counter-propagating light pulses. *Opt. Express* **2012**, *20*, 12877−12884.
(39) Kahl, P.; Podbiel, D.; Schneider, C.; Makris, A.; Sindermann, S.; Witt, C.; Kilbane, D.; Hoegen, M. H.-v.; Aeschlimann, M.; zu Heringdorf, F. M. Direct Observation of Surface Plasmon Polariton Propagation and Interference by Time-Resolved Imaging in Normal-Incidence Two Photon Photoemission Microscopy. *Plasmonics* **2018**, *13*, 239−246.
(40) Kim, H.-g.; Choi, H. J. Thickness dependence of work function, ionization energy, and electron affinity of Mo and W dichalcogenides from DFT and GW calculations. *Phys. Rev. B* **2021**, *103*, 085404.
(41) Cinchetti, M.; Oelsner, A.; Fecher, G. H.; Elmers, H. J.; Schönhense, G. Observation of Cu surface inhomogeneities by multiphoton photoemission spectromicroscopy. *Appl. Phys. Lett.* **2003**, *83*, 1503−1505.
(42) Aeschlimann, M.; Bauer, M.; Bayer, D.; Brixner, T.; García de Abajo, F. J.; Pfeiffer, W.; Rohmer, M.; Spindler, C.; Steeb, F. Adaptive subwavelength control of nano-optical fields. *Nature* **2007**, *446*, 301−304.
(43) Buckanie, N.; Kirschbaum, P.; Sindermann, S.; zu Heringdorf, F.-J. M. Interaction of light and surface plasmon polaritons in Ag Islands studied by nonlinear photoemission microscopy. *Ultramicroscopy* **2013**, *130*, 49−53.
(44) Tidy3D, the full-wave simulator employing the finite-difference time-domain (FDTD) method, developed by Flexcompute Inc. https://www.flexcompute.com/tidy3d/solver (accessed: 2024−10−24).
(45) Munkhbat, B.; Wróbel, P.; Antosiewicz, T. J.; Shegai, T. O. Optical Constants of Several Multilayer Transition Metal Dichalcogenides Measured by Spectroscopic Ellipsometry in the 300−1700 nm Range: High Index, Anisotropy, and Hyperbolicity. *ACS Photonics* **2022**, *9*, 2398−2407.
(46) Wu, Q.; Wang, L.; Zhang, H.; Deng, J.; Zhao, Y.; Liu, J.; Xiang, J.; Wu, S. Strong coupling of excitons in monolayer WS2 with guided-mode resonance. *Results in Physics* **2023**, *44*, 106191.
(47) Chahshouri, F.; Taleb, M.; Diekmann, F. K.; Rossnagel, K.; Talebi, N. Interaction of excitons with Cherenkov radiation in WSe2 beyond the non-recoil approximation. *J. Phys. D: Appl. Phys.* **2022**, *55*, 145101.
(48) Klick, A.; Großmann, M.; Beewen, M.; Bittorf, P.; Fiutowski, J.; Leißner, T.; Rubahn, H.-G.; Reinhardt, C.; Elmers, H.-J.; Bauer, M. Femtosecond time-resolved photoemission electron microscopy operated at sample illumination from the rear side. *Rev. Sci. Instrum.* **2019**, *90*, 053704.
(49) Buck, J.; Iwicki, J.; Rossnagel, K.; Kipp, L. Surface photovoltage effect at the p-WSe_2:Rb surface: Photoemission experiment and numerical model. *Phys. Rev. B* **2011**, *83*, 075312.

Downloaded from pubs.acs.org/apchd5/article-pdf/12/7/3484/4245906/1/ph5c00290.pdf by UNIV AUGSBURG user on 12 November 2026

https://doi.org/10.1021/acsphotonics.5c00290
ACS Photonics 2025, 12, 3484−3491